

A SEMI-PHYSICAL SIMULATION SYSTEM FOR DBF TRANSMITTER ARRAY ON LEO SATELLITE

G. Liang, W. B. Gong, H. J. Liu, and J. P. Yu

Shanghai Engineering Center for Microsatellites
Chinese Academy of Science
865 Changning Road, Shanghai 200050, China

Abstract—This paper presents a semi-physical simulation system for 61-channel DBF array transmitter antenna on LEO satellite. It consists of a hardware platform for digital beamforming network (BFN) and a software simulation system for DBF array. The background and wideband input interface are described, and the signal process of digital beamforming network is discussed in detail. General DFT filter bank, distributed arithmetic (DA) algorithm and Hartley image rejection structure are adopted to design the digital BFN, which make the calculation of BFN reduced by 98.41% and get the multiplier consumption decreased to 7.11%, compared with conventional algorithms. A novel digital BFN hardware platform with distributed structure is designed, which can complete the high speed array signal processing with maximum throughput of 32.025 Gbps. Ultimately, the measurements of semi-physical simulation system show good agreement with the ideal simulation result. The derivation of radiation pattern from energy distribution of earth's surface demonstrates that the DBF array has good performance on beam coverage with equal flux density and satisfies the application in mobile satellite communication.

1. INTRODUCTION

With the development of digital signal processing and software designed radio technologies, digital beamforming (DBF) array provides the most promising solution for future phased array antenna design. DBF array antenna has the capability of forming multi-beam simultaneously by dint of spatial filtering. Combined with CDMA and FDMA technologies, multi-beam array antenna can enhance the

Corresponding author: G. Liang (hnlg219@163.com).

system capacity of mobile satellite communication, thus DBF array is becoming an essential part of contemporary LEO satellites [1, 2].

DBF array has many advantages over analog beamforming method, whereas there are several technological challenges for the realization of a DBF array. One is high speed data processing to permit real-time operation, another is the rapid transfer of large amounts of data between the antenna elements and the digital beamforming computer [3, 4]. A 61-channel DBF transmitter array is presented in this paper, which can steer 16 beams simultaneously with an instantaneous bandwidth of 10 MHz. And the throughput of digital beamforming computer at input is $2 \times 300 \text{ MSPS} \times 12 = 7.2 \text{ Gbps}$, and the data transfer speed is $61 \times 37.5 \text{ MSPS} \times 14 = 32.025 \text{ Gbps}$. Therefore the main objective of BFN design is to reduce the computation and hardware resource consumption. Many algorithms such as DFT filter bank and distributed arithmetic are adopted to realize the goal, and a distributed digital beamforming network is designed to complete high speed signal processing of the 61 parallel channels, which can reduce the calculation by 98.41% and lessen the multiplier resource consumption to 7.11%.

2. BACKGROUND AND INTERFACE

The DBF array is designed for the application of mobile satellite communication [5]. As the phased array antenna scans in wide angle (in the region $[-53^\circ, 53^\circ]$), the variation of transmission loss in scan range can attain up to 7 dB. And the transmission loss of mobile satellite communication surrounding is mainly free space path loss, the mathematic formula of which is expressed as following

$$P_{\text{loss}}(\theta) = -10 \lg \left[\lambda^2 / (4\pi d)^2 \right] \text{ (dB)} \quad (1)$$

where λ is the wavelength of transmitting wave, and d is transmission distance of EMW, calculated as below

$$d = R_e \sin \left[\arcsin \left(\frac{R_e}{\sin \theta * (R_e + h)} \right) - \theta \right] / \sin \theta \quad (2)$$

where R_e is the radius of earth, h is height of satellite circle, θ is the scan angle [6].

The variation of transmission loss may lead to “near and far effect” in CDMA standard, which is usually applied in mobile satellite communication. To reduce the design difficulty of power control in satellite payload, the DBF array antenna with equal flux coverage is taken into consideration. The average main lobe level of beams on the periphery of beam coverage (sixteen beams) should be higher than

that of the center beam, which can compensate for the vibration of transmission loss [7, 8].

The input of digital BFN is fed by two channels of wideband analog signals (with 120 M bandwidth), each of which consists of eight beams with an instantaneous bandwidth of 10 MHz individually. The center frequency of each beam is arranged as following:

$$f_k = 12.5 * k \text{ (MHz)}, k = 1, 2, \dots, 8 \tag{3}$$

The distribution of 16 beams' frequency spectrum is depicted as Fig. 1. The phase and amplitude adjustment of 16 beams are controlled precisely in the digital BFN, and the phase and amplitude adjustment coefficients are calculated previously by nonlinear optimization algorithms [9]. The 16 beams are synthesized simultaneously into 61 channels and transformed to analog signals. Then 61-channel signals are up-converted to transmitting frequency (*S* band) by 61 RF front-ends, and finally transmitted by radiating elements [10].

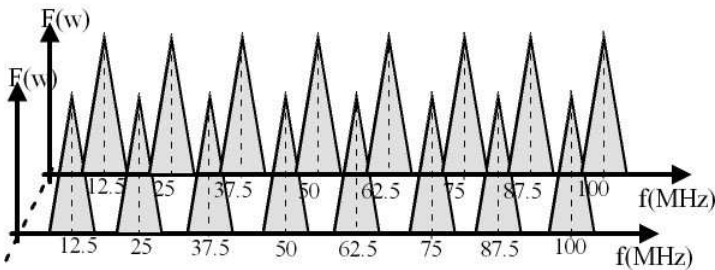


Figure 1. Frequency distribution of sixteen beams.

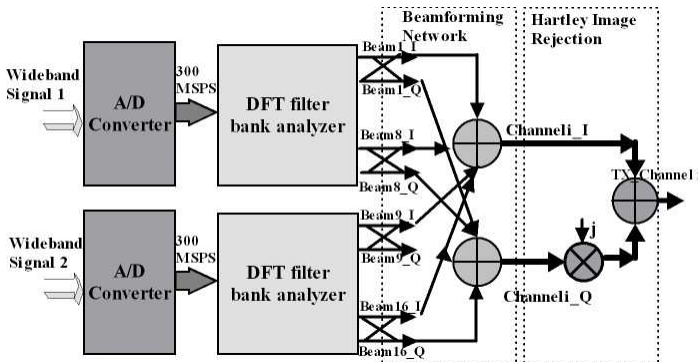


Figure 2. Block diagram of digital BFN (one TX channel).

3. SIGNAL PROCESSING OF DIGITAL BFN

The detail of interface has been described in Section 2, two-channel wideband signals with 120 MHz bandwidth are transferred to the input of digital beamforming network, each of which is divided into 8 subchannels. And each subchannel is taken up by one beam individually with an instantaneous bandwidth of 10 MHz.

The block diagram of digital BFN is shown in Fig. 2, one transmitting channel is merely illuminated. First, two wideband channels are band-pass sampled by AD converters with a 300 MHz sample clock. Two general DFT filter bank analyzers are adopted to divide the sixteen beams from two wideband signals. The K -channel outputs of DFT filter bank analyzers are the divided complex signals of 16 beams. As the DFT filter bank analyzer is high efficient realization of quadrature down-conversion, the orthogonal transform is also completed. The real and image parts of each complex output are the I and Q extraction of each beam respectively. The complex signals of 16 beams are transferred to beamforming computer, where the phase and amplitude adjustment are put into practice. Since the beam coverage is fixed, the phase and amplitude excitation coefficients were calculated previously by Genetic Algorithm according to the predefined radiation patterns [11–14]. Hartley image-rejection structure is designed to eliminate the overlapping image frequency caused by DFT filter bank analyzer. The detail of DFT filter bank, beamforming computer and Hartley image-rejection structure will be described in detail.

3.1. General DFT Filter Bank Analyzer

The original mathematic model of general DFT filter bank analyzer with K -channel outputs is quadrature down-conversion, shown in Fig. 3.

The wideband input signal $x(n)$ is modulated by the LO signals with function $W_K^{kn} = e^{-j2\pi kn/K}$, $k = 0, 1 \dots K$, then filtered by N -order low-pass or band-pass filter $h(n)$ to eliminate other beams' frequency spectrum. As the bandwidth of the k -th channel decreases, decimation is adopted, M is the decimation factor. Therefore, the k -th channel output $x_k(m)$ is expressed as

$$x_k(m) = \sum_{n=0}^{N-1} [x(n)W_K^{kn}] \cdot h(mM - n) \quad (4)$$

Let n be expressed as $n = rK - \rho$, $\rho \in [0, \dots K - 1]$, $r \in [0, \dots \frac{N-K}{K}]$,

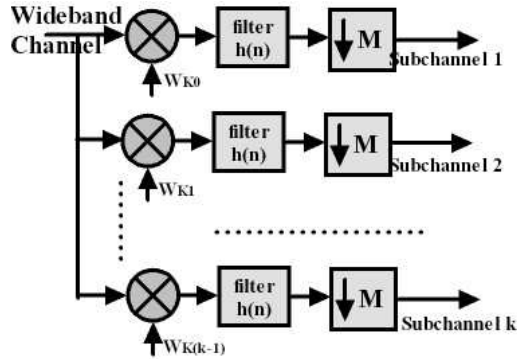


Figure 3. The original model of general DFT filter bank.

applied in Eq. (4)

$$x_k(m) = \sum_{r=0}^{(N-K)/K} \sum_{\rho=0}^{K-1} h(mM - rK + \rho) \cdot x(rK - \rho) \cdot W_K^{-k\rho} \quad (5)$$

Define $x_\rho(r) = x(rK - \rho)$, it denotes that the input signal $x(n)$ is delayed by ρ sample time and then decimated by K times. The number of channels K is I times of decimation rate M , $K = MI$. So Eq. (5) can be expressed as

$$x_k(m) = \sum_{r=0}^{(N-K)/K} \sum_{\rho=0}^{K-1} h((m - rI)M + \rho) \cdot x_\rho(r) \cdot W_K^{-k\rho} \quad (6)$$

Define $P_\rho(m) = h(mM + \rho)$, $\rho = 0, \dots, K - 1$ further, it denotes that the impulse response of filter $h(n)$ is delayed by ρ sample time and then decimated by M times. Applying the definition to Eq. (6)

$$\begin{aligned} x_k(m) &= \sum_{r=0}^{(N-K)/K} \sum_{\rho=0}^{K-1} P_\rho(m - rI) \cdot x_\rho(r) \cdot W_K^{-k\rho} \\ &= \sum_{\rho=0}^{K-1} W_K^{-k\rho} \left[\sum_{r=0}^{(N-K)/K} P_\rho(m - rI) \cdot x_\rho(r) \right] \end{aligned} \quad (7)$$

Let $y_\rho(m)$ be expressed as

$$y_\rho(m) = \sum_{r=0}^{(N-K)/K} P_\rho(m - rI) x_\rho(r) \quad (8)$$

Define $l = rI$, and apply it to Eq. (8)

$$y_\rho(m) = \sum_{l=0}^{N/M-1} P_\rho(m-l)x_\rho(l/I) \tag{9}$$

where $x_\rho(m/I)$ is the interpolation result of $x_\rho(m)$ by I times, defined as $x'_\rho(l)$. So that Eq. (9) can be expressed as

$$y_\rho(m) = \sum_{m=0}^{N/M-1} P_\rho(m) * x'_\rho(m) \tag{10}$$

Note that $y_\rho(m)$ is the filter result of $x'_\rho(m)$ filtered by polyphase filter $P_\rho(m)$. Applying Eq. (10) to Eq. (7)

$$x_k(m) = \sum_{\rho=0}^{K-1} y_\rho(m)W_K^{-k\rho} = \sum_{\rho=0}^{K-1} y_\rho(m)(W_K^*)^{k\rho} \tag{11}$$

We can see that the k -th channel output $x_k(m), k = 0, 1, \dots, K - 1$ is the K -point Discrete Fourier Transform result of $y_\rho(m), \rho = 0, 1, \dots, K - 1$ inferred in Eq. (10). And the real and image part of the $x_k(m)$ is the I and Q extraction of the k -th beam. When $K = M$, it can be called as critically sampled DFT filter bank. The block diagram of polyphase realization structure for general DFT filter bank analyzer is shown in Fig. 4.

Because the filter and DFT is arranged after decimation, the computation should be reduced by M times. 2-point Decimation-In-Time FFT algorithm can be adopted to complete the DFT, and its butterfly structure could reduce computation further. The ρ -th polyphase branch $P_\rho(m)$ is the decimation result of original filter $h(n)$, and the sum of coefficients for K polyphase branches $P_\rho(m)$ is

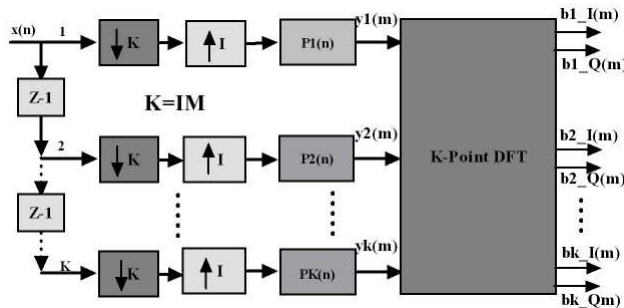


Figure 4. Block diagram of general DFT filter bank analyzer.

Table 1. The comparison between DFT filter bank and quadrature down-conversion structure.

Algorithm	Calculation (complex multiplying/s)	Multiplier
DFT filter bank	$(N + K \cdot \log_2 k) \cdot F/M$	$N + K \cdot \log_2 k/2$
Quadrature down-conversion	$(N + 1) \cdot K \cdot F$	$(N + 1) \cdot K$
Remark: F is the sample rate of input signal; 2-pont DIT- FFT algorithm is adopted		

N -order. It is equal to that for original filter $h(n)$, which reduces the consumption of multiplier implemented on filter by K times. The comparison between DFT filter bank and original quadrature down-conversion structure in terms of calculation and consumption of multiplier is given in Table 1 [10, 11].

Because the resolving capability of DFT in digital domain is $2\pi/K$, and the frequency distance of adjacent beam is 12.5 MHz (the sample rate is 300 MHz), a 24-channel DFT filter bank with decimation factor $M = 8$ is designed. And a band-pass filter is proposed, with the characteristic exhibited as following

$$\begin{cases} f_{\text{stop1}} = 5 \text{ M} \\ f_{\text{stop2}} = 20 \text{ M}, \delta = 80 \text{ db} \\ f_{\text{pass1}} = 7.5 \text{ M}, \delta = 60 \text{ db} \\ f_{\text{pass2}} = 17.5 \text{ M} \end{cases} \quad (12)$$

So the sample rate of 24-channel DFT filter bank output reduces to 37.5 MHz, with center frequency 12.5 MHz. Since the number of beam in one wideband channel is 8, we can choose merely the $k = 0, 1, \dots, 7$ channel output of DFT filter bank, which can reduce the calculation of FFT further [12].

3.2. Digital Beamforming Computer

After DFT filter bank, the complex signals of 16 beams are divided from two wideband channels, and fed to digital beamforming network. They can be expressed as

$$\overrightarrow{B_{1 \times 16}} = \left[\overrightarrow{B_1(n)}, \overrightarrow{B_2(n)}, \dots, \overrightarrow{B_{16}(n)} \right] \quad (13)$$

The beamforming matrix of DBF network is

$$R_{16,61} = \begin{bmatrix} R_{1,1} & R_{1,2} & \dots & R_{1,61} \\ R_{2,1} & \dots & \dots & R_{2,61} \\ \dots & \dots & \dots & \dots \\ R_{16,1} & \dots & \dots & R_{16,61} \end{bmatrix}_{16 \times 61} \quad (14)$$

where the cell $R_{i,j}$ denotes the amplitude and phase adjusting coefficient of the i -th beam excited by the j -th channel. The output results of DBF network will be transferred to 61 RF front-end channels, expressed as vector: $[\overline{T_1(n)}, \overline{T_2(n)}, \dots, \overline{T_{61}(n)}]$. The j -th channel signals are calculated as following:

$$\overline{T_j(n)} = \sum_{i=1}^{16} \overline{B_i(n)} * \overline{R_{i,j}} \quad (15)$$

It can be concluded that DBF network needs 3904 multipliers to complete the 61 channels' rapid beamforming calculation of 16 beams. The limitation of multipliers resource in ASIC becomes the key point of BFN design. So distributed arithmetic (DA) algorithm is adopted to fulfill the high-speed parallel calculation of BFN, which require large-amount multiplier consumption. DA algorithm is fit for multiplying with fixed coefficients. Instead of utilizing hardware multiplier, memory can be configured as look-up-table (LUT) to realize the multiplying computation, which is considered as software multiplier. The principles of DA algorithm are demonstrated as following.

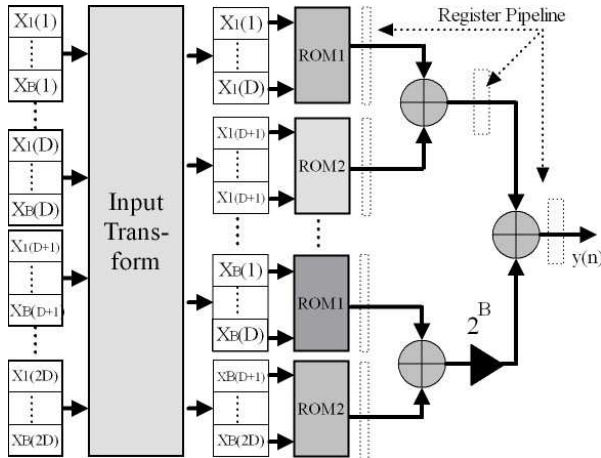


Figure 5. Block diagram of DA algorithm.

N fixed coefficients $c(n)$ multiply with input signal $x(n)$, and the multiply-and-sum result $y(n)$ can be expressed as

$$y = \sum_{n=1}^N c(n) \cdot x(n) = c(1) \cdot x(1) + c(2) \cdot x(2) + \dots + c(n) \cdot x(n) \quad (16)$$

And the input signal $x(n)$ is quantified as binary digit, expressed as

$$x(n) = -2^{B-1} \cdot x_B(n) + \sum_{b=1}^{B-1} x_b(n) \cdot 2^{b-1} \quad (17)$$

where B is the bits number of $x(n)$, and $x_b(n)$ is the b -th bit of $x(n)$. Applying Eq. (17) to Eq. (16), we can see that

$$\begin{aligned} y &= \sum_{n=1}^N c(n) \cdot (-2^{B-1} \cdot x_B(n) + \sum_{b=1}^{B-1} x_b(n) \cdot 2^{b-1}) \\ &= c(1)(-x_B(1) \cdot 2^{B-1} + x_{B-1}(1) \cdot 2^{B-2} + \dots + x_1(1) \cdot 2^0) \\ &\quad + c(2)(-x_B(2) \cdot 2^{B-1} + x_{B-1}(2) \cdot 2^{B-2} + \dots + x_1(2) \cdot 2^0) \\ &\quad + \dots + c(N)(-x_B(N) \cdot 2^{B-1} + x_{B-1}(N) \cdot 2^{B-2} + \dots + x_1(N) \cdot 2^0) \\ &= -(c(1) \cdot x_B(1) + c(2) \cdot x_B(2) + \dots + c(N) \cdot x_B(N)) \cdot 2^{B-1} \\ &\quad + (c(1) \cdot x_{B-1}(1) + c(2) \cdot x_{B-1}(2) + \dots + c(N) \cdot x_{B-1}(N)) \cdot 2^{B-2} \\ &\quad + \dots + (c(1) \cdot x_1(1) + c(2) \cdot x_1(2) + \dots + c(N) \cdot x_1(N)) \cdot 2^0 \quad (18) \end{aligned}$$

All the possibilities of coefficients' sum in brackets (in Eq. (18)) can be stored in memory which is configured as Look-Up-Table structure. Utilizing the vector $[x_b(N), x_b(N-1), \dots, x_b(1)]$ as Look-Up-Table address, the output of Look-Up-Table is multiplied by 2^b , $b = 0, 1 \dots B-1$, and the multiplying can be realized by shifter. Finally, the sum of shifted result is $y(n)$. The same bit of 16 beams is combined into the address vector $[x_b(N), x_b(N-1), \dots, x_b(1)]$, which is similar with transpose of matrix [13]. The block diagram of beamforming computer is depicted in Fig. 5.

3.3. Hartley Image Rejection Structure

Because the original model of DFT filter bank is quadrature down-conversion, the aliasing frequency occurs in the analyzer. Take the k -th channel for example, it is modulated by LO signals e^{-jw_0n} , the I exaction of the k -th beam $I(n)$, whose frequency spectrum can be expressed as $I(w) = \frac{F(w+w_0)+F(w-w_0)}{2}$; and the frequency spectrum of Q exaction can be expressed as $Q(w) = \frac{F(w+w_0)-F(w-w_0)}{2j}$, where $F(w)$ is the w frequency spectrum of wideband input signal.

For example, the fourth channel of DFT filter bank ($k = 3$) is aliased with the second beam, that is the image frequency of the second beam overlapped with the down-converted frequency of the fourth beam. It can be conclude that the k -th beam will be aliased with the $|k - 2|$ beam, as the center frequency of filter is at 12.5 MHz ($k = 1$). If we adopt the low-pass filter, the aliasing frequency can't be cancelled, because of the asymmetry property of each beam's spectrum [14, 15].

Because the phase excitation coefficients are constants, the aliasing frequency still exists. After beamforming, the new I extraction $I'(n)$ and Q extraction $Q'(n)$ of some beam are expressed as

$$I' + jQ' = (I + jQ) \times Ae^{j\theta} A(I \cos \theta - Q \sin \theta) + jA(I \sin \theta + Q \cos \theta) \quad (19)$$

where $Ae^{j\theta}$ is phase excitation coefficient, and the frequency spectrum of $I'(n)$ and $Q'(n)$ can be expressed as

$$\begin{cases} I'(w) = A \left[\frac{F(w+w_0)+F(w-w_0)}{2} \cos \theta - \frac{F(w+w_0)-F(w-w_0)}{2j} \sin \theta \right] \\ Q'(w) = A \left[\frac{F(w+w_0)+F(w-w_0)}{2} \sin \theta + \frac{F(w+w_0)-F(w-w_0)}{2j} \cos \theta \right] \end{cases} \quad (20)$$

Hartley image rejection structure is designed to eliminate the aliasing frequency and reconstruct the sixteen beams signal. The Q channel signals $Q'(n)$ multiply with j and then add I channel signal $I'(n)$. The reconstructed signal are calculated like below

$$T(n) = I'(n) + j * Q'(n) \quad (21)$$

Define $U = AF(w + w_0)$, $V = AF(w - w_0)$, applied to Eq. (21). The frequency spectrum of reconstructed signal can be expressed as

$$\begin{aligned} T(w) &= \left[\left(\frac{U + V}{2} \right) \cos \theta - \frac{U - V}{2j} \sin \theta \right] \\ &+ j \left[\left(\frac{U + V}{2} \right) \sin \theta + \frac{U - V}{2j} \cos \theta \right] \\ &= \left(\frac{U + V}{2} + \frac{U - V}{2} \right) \cos \theta + j * \left(\frac{U + V}{2} + \frac{U - V}{2} \right) \sin \theta \\ &= U (\cos \theta + j \sin \theta) = Ue^{j\theta} \end{aligned} \quad (22)$$

We can see that the aliasing frequency has been eliminated completely by Hartley image rejection structure, and it has no influence on the precision of beamforming network. Multiplying with j can be realized by Hilbert Transform. Because $Q'(n)$ is band-passed signals, III type Hilbert Transformer with odd symmetry property is adopted. To reduce the multiplier resource consumption, Hilbert Transformer with half-band characteristic is proposed further. However, the

positive part of frequency spectrum is multiplied by $-j$ by utilizing Hilbert Transformer in time domain. Therefore, after the Q channel signals pass through Hilbert Transformer, they should minus I channel signals [16, 17].

4. SIMULATION AND HARDWARE IMPLEMENTATION

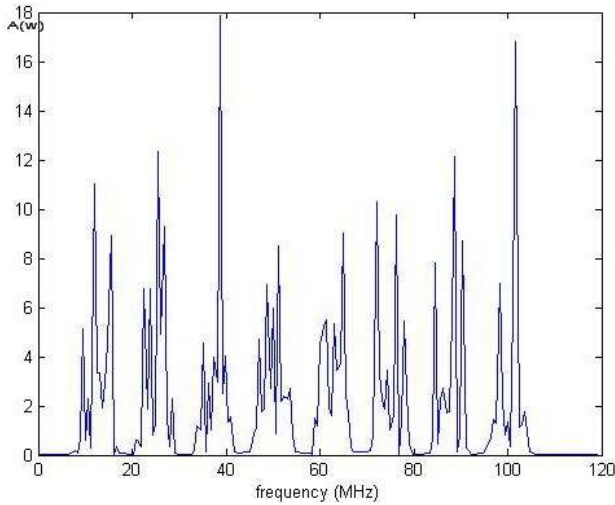


Figure 6. The spectrum of one wideband input signal.

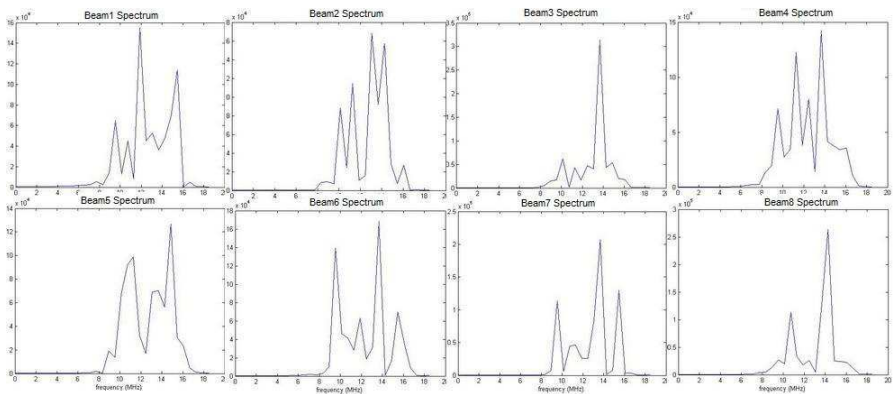


Figure 7. The spectrum of of 8 reconstructed beams.

To validate the feasibility of algorithms discussed above, the algorithms are simulated by the aid of MATLAB, and the simulation result is presented in Figs. 6 and 7. One wideband signal (120 M bandwidth) is driven to DFT filter bank, where frequency division and orthogonal transform of 8 beams are completed. Then the signals are transferred to Hartley image rejection unit to eliminate the aliasing frequency, on the assumption that all the phase excitation coefficients are zero. 8 reconstructed beams is shown in Fig. 7.

Ultimately, a hardware platform of digital BFN was designed, the photograph of which is shown in Fig. 8. Distributed process architecture is adopted to complete the high speed array signal processing with maximum throughput 32.025 Gbps, FPGA (Field Programmable Gate Array) is adopted to design the DBF network hardware platform, as other architecture chips such as DSPs can't provide such high speed processing power. FPGA consists of DSP Block, Block RAM and LE resource, which can be configured as hardware multiplier and software multiplier to satisfy multiplier-and-sum demand of digital beamforming unit. Its reconfiguration capability provides the possibilities of DBF array's in-orbit reconfiguration, which could make phased array antenna change radiation pattern flexibly [18].

The algorithms are quantified and transplanted into FPGA, and the resource consumption of algorithms is exhibited in Table 2. From Table 2, we can draw the conclusion that the proposed algorithms can reduce the computational complexity, resource consumption, and make hardware implemented with ease. Compared with conventional



Figure 8. Photograph of semi-physical simulation platform (including digital BFN hardware platform).

Table 2. The comparison between algorithm in BFN and corresponding conventional algorithms.

Module	Algorithm	Multiplier	Computation (MIPS)
Orthogonal transform	DFT filter bank	552	20700
	Quadrature down-conversion	3856	1156800
Beamforming computer	Original computer	3904	146400
	DA algorithm	0	0 (but 2287.5 Look-up operation)
Remark	Utilizing 240-order filter, FFT based on 2-point algorithm		

algorithms, the computation of BFN can be reduced by 98.41% and resource consumption can be reduced to 7.11%, which lays a foundation for the future space application.

5. SEMI-PHYSICAL SIMULATION

A semi-physical simulation platform is designed to evaluate the effect of digital beamforming network. Its interconnect architecture is depicted in Fig. 8. First, two wideband signals with the property described in Section 2, are generated by signal generator, which works as access unit in satellite payload. The two-channel signals are transferred to hardware platform of digital beamforming network, which performs the functions of DFT filter bank, beamforming computer and image rejection. According to the algorithms discussed above, sixteen beams are synthesized into 61 channels. The 61-channel digital signals are fed to the buffer, and then transferred to PC by USB 2.0 interface. We design a software simulation system for DBF array antenna on LEO satellite, which can simulate the work condition of phased array antenna in space and the process of transmitting 61-channel signals. The operating environment of software simulation system is shown in Fig. 9. The basic mathematic model of DBF array on LEO satellite is presented like this. First the 61-channel received data are separated by software simulation system according to the predefined frame format, they are the transmitting signals of DBF array, expressed as vector

$$\overrightarrow{I(n)} = [[\overrightarrow{I_1(n)}, \overrightarrow{I_2(n)}, \dots, \overrightarrow{I_{61}(n)}]]^T, \overrightarrow{I_i(n)} \in C \quad (23)$$

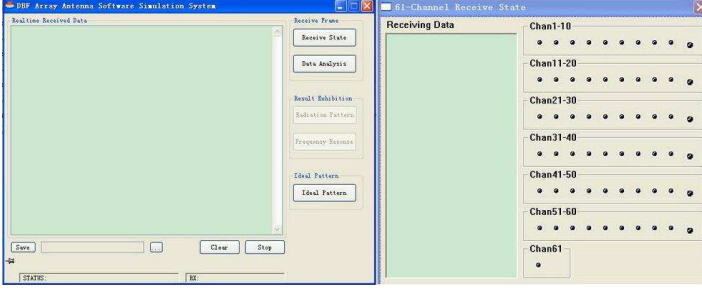


Figure 9. Operating environment windows of software simulation system.

Let's establish the coordinate system for the planar array antenna with the coordinate origin in its physics center. A standard hexagonal array (SHA) with 61 elements is recommended for the application in mobile satellite communication. The 61-channel separated data is radiated by the 61 elements respectively, and propagates in space. The propagation delay of 61-channel transmitting signals at specific direction is given by

$$\vec{D}_{1 \times 61} = \left[e^{-j(x_1 \sin \theta \cos \varphi + y_1 \sin \theta \sin \varphi) / \lambda}, e^{-j(x_2 \sin \theta \cos \varphi + y_2 \sin \theta \sin \varphi) / \lambda}, \dots, e^{-j(x_{61} \sin \theta \cos \varphi + y_{61} \sin \theta \sin \varphi) / \lambda} \right] \quad (24)$$

where λ is the wavelength, $[x_i, y_i]$ is the coordinates of the i -th element, θ is elevation angle, φ is azimuth angle.

Therefore the far-field radiation pattern produced by planar array can be expressed as

$$D(\theta) = 10 \lg \left(\left| \sum_{n=1}^N \sum_{i=1}^{61} \left(\overrightarrow{I_i(n)} \cdot e^{-j(x_i \sin \theta \cos \varphi + y_i \sin \theta \sin \varphi) / \lambda} \right) / N \right|^2 / 61 \right) + P(\theta) \quad (25)$$

where $P(\theta)$ represents the radiation pattern of each individual element, and N is the sample number of each channel. From Eq. (25), we can see that the radiation pattern is calculated by dint of cumulative energy of actual transmitting signals [24–26].

To validate the precision of BFN, the predicted performance is shown below, which was computed by using conventional ideal model for phased array antenna without real signal processing. And the predicted pattern match well with the semi-physical simulation result, they are depicted in Figs. 10 and 11.

The sixteen predefined beams are arranged in three circles, six beams in the second circle, the rest in third circle, which is similar with the beam coverage of Global Star System. From Figs. 10 and 11, we can see that the semi-physical simulation result show good agreement with the predicted pattern, and digital beamforming network has exceptional performance. The gain variance δ^2 between the predicted pattern (normalized) and semi-physical simulated pattern (normalized)

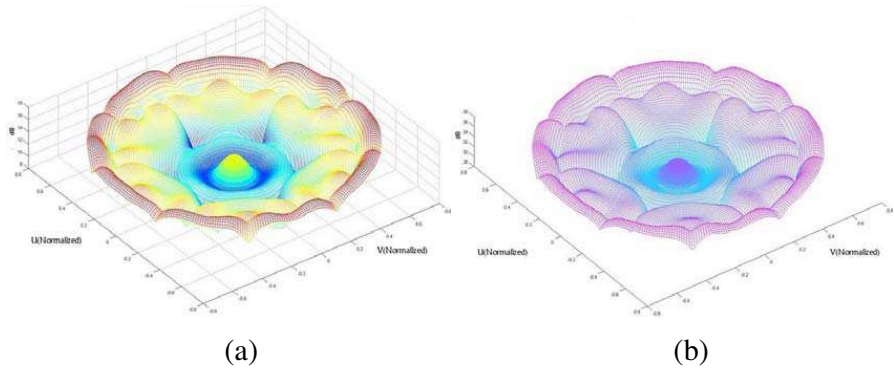


Figure 10. The comparison of three-dimensional radiation pattern: (a) Predicted pattern; (b) Semi-physical simulation.

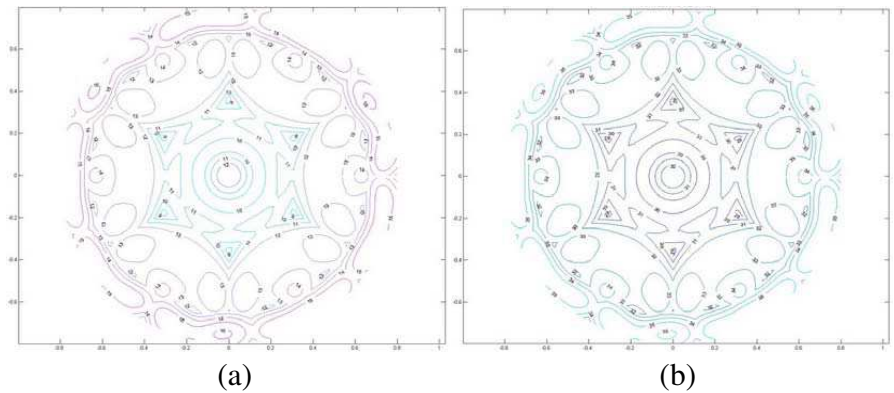


Figure 11. The comparison of radiation pattern's contour map: (a) Predicted pattern; (b) Semi-physical simulation.

is 0.1297, which is computed in accordance with Eq. (26)

$$\delta^2 = \sum_{i=0}^M \sum_{j=0}^N \{ [G_p(\theta_i, \varphi_j) - \max(G_p(\theta_i, \varphi_j))] - [G_s(\theta_i, \varphi_j) - \max(G_s(\theta_i, \varphi_j))] \}^2 / (MN) \quad (26)$$

where $G_p(\theta_i, \varphi_j)$ represents the predicted gain at specific direction (θ_i, φ_j) , and $G_s(\theta_i, \varphi_j)$ represents that of the semi-physical simulated result. M and N represent the sample number of θ and φ respectively. The pattern gain error is mainly caused by the quantification error of DBF network.

The transmission loss is deducted from the semi-physical simulated pattern, then we can get the true gain distribution of earth’s surface. Applying Eq. (1) to Eq. (25), the true gain distribution is given by

$$D'(\theta) = 10 \lg \left(\left| \sum_{n=1}^N \sum_{i=1}^{61} \overrightarrow{I_i(n)} \cdot e^{-j(x_i \sin \theta \cos \varphi + y_i \sin \theta \sin \varphi) / \lambda} / N \right|^2 / 61 \right) + P(\theta) + P_{\text{loss}}(\theta) \quad (27)$$

The section map of the true gain distribution of earth’s surface ($\varphi = 0$) is shown in Fig. 12.

In entire scan range from -53° to 53° , the maximum gain fluctuation is 1.2 dB, which takes place at center beam. The gain variation in the other region is below 1 dB. It can be concluded that the predefined radiation pattern of DBF array enjoys the capability of equal flux density coverage, which can compensate for the transmission loss efficiently.

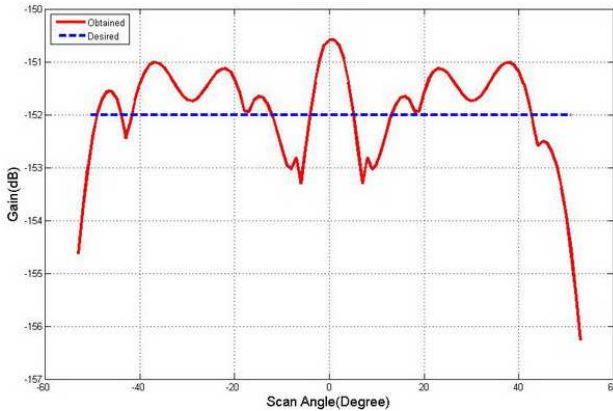


Figure 12. The section map of the true gain distribution of earth’s surface ($\varphi = 0$).

6. CONCLUSION

An initial demonstration of 61-channel DBF transmitter array antenna for mobile satellite communication is presented in this paper. The background of wide-angle scannable DBF array on LEO satellite, with varying in transmission loss, requires the beamforming of DBF array to be equipped with equal flux density coverage. The wideband input interface and signal processing of digital beamforming network are discussed in detail. A distributed beamforming network based on DFT filter bank, distributed arithmetic and Hartley image rejection structure is designed to complete the high speed array signal processing with maximum throughput of 32.025 Gbps. Ultimately, a semi-physical simulation platform is designed, the measurements of which show good agreement with the ideal simulation result. The radiation pattern, computed by energy cumulation of real transmitting signal, demonstrates that the DBF array has good performance on equal flux density coverage.

REFERENCES

1. Roy, S. D. and S. Kundu, "Performance analysis of cellular CDMA in presence of beam forming and soft soft hand off," *Progress In Electromagnetics Research*, PIER 88, 73–89, 2008.
2. Chiba, I., R. Miura, and T. Tanaka, "Digital beam forming (DBF) antenna system for mobile communications," *IEEE Transactions on Aerospace and Electronic Systems*, Vol. 12, No. 9, 31–41, 1997.
3. Athanasopoulos, N. C. and N. K. Uzunoglu, "Development of a 10 GHz phased array cylindrical antenna system incorporating IF phase processing," *Progress In Electromagnetics Research*, PIER 59, 17–38, 2006.
4. Kuwahara, Y., H. Kakinuma, and S. Ogawa, "Development and evaluation test of DBF equipment for transmitting," *IEEE AP-S1999*, Florida, USA, 1999.
5. Dreher, A., N. Niklasch, and F. Klefenz, "Antenna and receiver system with digital beam forming for satellite navigation and communications," *IEEE Transactions on Microwave Theory and Techniques*, Vol. 51, No. 7, 1815–1821, 2003.
6. Rappaport, T. S., *Wireless Communications Principles and Practice*, Publishing House of Electronics Industry, Beijing, 2004.
7. Lu, Z.-Y., "Design method of the ring-focus antenna with a variable focal distance for forming an elliptic beam," *Progress In Electromagnetics Research Letters*, Vol. 4, 73–80, 2008.

8. Reyna, A. and M. A. Panduro, "Optimization of a scannable pattern for uniform planar antenna arrays to minimize the side lobe level," *Journal of Electromagnetic Waves and Application*, Vol. 22, No. 16, 2241–2250, 2008.
9. Rostami, A. and A. Yazdanpanah-Goharrizi, "Hybridization of neural networks and genetic algorithms for identification of complex Bragg gratings," *Journal of Electromagnetic Waves and Application*, Vol. 22, No. 5–6, 643–664, 2008.
10. Curtis, D. D. and R. W. Capt, "32-Channel X-Band digital beamforming plug-and-play receive array," *IEEE Symposium on Phased Array Systems and Technology*, Boston, USA, 2003.
11. Xu, Z., H. Li, Q.-Z. Liu, and J.-Y. Li, "Pattern synthesis of conformal antenna array by the hybrid genetic algorithm," *Progress In Electromagnetics Research*, PIER 79, 75–90, 2008.
12. Mahanti, G. K. and A. Chakrabarty, "Phase-only and amplitude-phase only synthesis of dual-beam pattern linear antenna arrays using floating-point genetic algorithms," *Progress In Electromagnetics Research*, PIER 68, 247–259, 2007.
13. Zhou, S. G., B. H. Sun, J. L. Guo, Q. Z. Liu, and Y. Hua, "A new fitness function for optimizing the matching network of broadband antennas by genetic algorithm," *Journal of Electromagnetic Waves and Application*, Vol. 22, No. 5–6, 759–765, 2008.
14. Kouveliotis, N. K., S. C. Panagiotou, P. K. Varlamos, T. D. Dimousios, and C. N. Capsalis, "Optimizing a PIFA using a genetic algorithms approach," *Journal of Electromagnetic Waves and Application*, Vol. 22, No. 2–3, 453–461, 2008.
15. Crochiere, R. E. and L. R. Rabiner, *Multirate Digital Signal Processing*, Prentice-Hall Press, New Jersey, 2001.
16. Nalbalwar, S., S. D. Joshi, and R. K. Patney, "A novel approach to design of signal matched QMF and DFT filter bank," *IEEE 15th International Conference on Software Telecommunications and Computer*, Darmstadt, Germany, 2007.
17. Karp, T., M. Kieffer, and P. Duhamel, "Parity-check matrix calculation for paraunitary oversampled DFT filter banks," *IEEE Transaction on Signal Processing*, Vol. 56, No. 10, 5277–5283, 2008.
18. Basese, U. M., *Digital Signal Processing with Field Programmable Gate Array*, Qinghua Press, Beijing, 2006.
19. Meng, C. C. and T. H. Wu, "2.4/5.7 GHz CMOS dual-band low-IF architecture using weaver-hartley image-rejection techniques," *IEEE Transaction on Microwave Theory and Techniques*, Vol. 57,

- No. 3, 552–556, 2009.
20. Zhang, X., Z. Wang, and D. Xu, “Wavelet packet transform-based least mean square beamformer with low complexity,” *Progress In Electromagnetics Research*, PIER 86, 291–304, 2008.
 21. Lyons, R. G., *Understanding Digital Signal Processing*, China Machine Press, Beijing, 2006.
 22. Lim, Y. C. and Y. J. Yu, “Optimum masking levels and coefficient sparseness for Hilbert transformers and half-band filters designed using the frequency-response masking technique,” *IEEE Transaction on Circuits and Systems*, Vol. 52, No. 11, 2444–2453, 2005.
 23. Panduro, M. A. and C. Bocio, “Design of beam-forming networks for scannable multi-beam antenna arrays using corps,” *Progress In Electromagnetics Research*, PIER 84, 173–188, 2008.
 24. Qu, Y., G. Liao, and S. Q. Zhu, “Pattern synthesis of planar antenna array via convex optimization for airborne forward looking radar,” *Progress In Electromagnetics Research*, PIER 84, 1–10, 2008.
 25. Svezhentsev, A. Y., “Some far field features of cylindrical microstrip antenna on an electrically small cylinder,” *Progress In Electromagnetics Research B*, Vol. 7, 223–244, 2008.
 26. Sukharevsky, O. I. and A. Y. Shramkov, “High-frequency method of antenna directional pattern calculation,” *Journal of Electromagnetic Waves and Application*, Vol. 21, No. 14, 2009–2023, 2007.